CELL BIOLOGY

BIG1/Arfgef1 and Arf1 regulate the initiation of myelination by Schwann cells in mice

Yuki Miyamoto,[1,2]* Tomohiro Torii,[3]* Kenji Tago,[4] Akito Tanoue,[2] Shou Takashima,[5] Junji Yamauchi[1,2]†

During development of the peripheral nervous system in mammals, Schwann cells wrap their plasma membranes around neuronal axons, forming multiple myelin sheaths. A mature myelin sheath insulates axons and increases nerve conduction velocity while protecting nerve fibers from various stresses such as physical ones. Despite this functional importance, the molecular units that underlie dynamic morphological changes in formation of myelin sheaths are not sufficiently understood. Arf1 is a small guanosine triphosphate–binding protein that plays multiple roles in intracellular trafficking and related signaling, both of which are processes involved in cell morphogenesis. We demonstrate that the Arf1 guanine nucleotide exchange factor, brefeldin A–inhibited guanine nucleotide-exchange protein 1 (BIG1)/Arfgef1, and the effector Arf1 regulate the initiation of myelination of axons by Schwann cells. Schwann cell–specific BIG1 conditional knockout mice, which have been generated here, exhibit reduced myelin thickness and decreased localization of myelin protein zero in the myelin membrane, compared with their littermate controls. BIG1 knockout mouse nerves specifically decrease the amounts of Arf1 in the AP1 clathrin adaptor protein subunits but not the Arf1 binding to GGA1 (Golgi-localized, gamma-adaptin ear-containing, Arf-binding protein 1) transporting proteins. The amounts of Arf1 in the COPI coatomer protein subunits were comparable in the knockout mice and controls. Similar results in myelin thickness are observed in Arf1 conditional knockout mice, which have also been generated here. Thus, the BIG1 and Arf1 unit plays a key role in Schwann cell myelination, newly adding it to the list of molecular units controlling myelination.

INTRODUCTION

During embryonic development of the peripheral nervous system in mammals, Schwann cell lineage cells migrate along peripheral neuronal axons from the dorsal to the ventral direction, arriving at their final destinations such as the limbs. After birth, they begin to wrap around individual axons and myelinate axons until ~2 months. Mature myelin sheaths play essential roles not only in insulating axons to increase nerve conduction velocity but also in protecting them from various external stresses such as physical ones. In the peripheral nervous system, myelin sheaths are derived from Schwann cells' morphologically differentiated plasma membranes. They often grow to more than 100 times larger than the collective surface areas of the premyelinating Schwann cell plasma membranes (*1*–*5*). As such, whereas myelin functions have been well studied, molecular units controlling the Schwann cells as they undergo such dynamic morphological changes, especially at the intracellular level, are not sufficiently understood.

Intracellular signaling molecules that control cell morphological changes involve a family of small guanosine triphosphatases (GTPases). They are active when bound to guanosine triphosphate (GTP) and are inactive when bound to guanosine diphosphate (GDP). Two regulatory molecules that are needed to behave like GTPases are signaling switches. Guanine nucleotide exchange factors (GEFs) replace GDP with free cytoplasmic GTP on GTPases to generate active GTPases. In contrast, GTPase-activating proteins promote intrinsic GTPase activities to generate inactive ones (*6*–*11*). Thus, a rate-limiting step to activate GTPases is thought to lie in their cognate GEFs.

Being representative of Ras family small GTPases, Arf family proteins also function as molecular switches (*2*–*9*). Arf proteins are widely expressed in tissues and are known to control cell morphological changes through the regulation of intracellular transporting proteins and related signaling (*6*–*9*). Among Arf proteins, Arf1 is well characterized and plays multiple roles in cells, as does Arf6 (*12*–*15*). For example, Arf1 assembles AP1 clathrin adaptor protein subunits and participates in the sorting of proteins from the trans-Golgi network (*16*–*18*). Also, Arf1 binds Golgi-localized, γ-adaptin ear-containing, Arf-binding proteins (GGAs), such as GGA1, and primarily regulates intracellular transport between the trans-Golgi network and the lysosome (*19*). Arf1 is also important for the assembly of COPI coatomer protein subunits and controls a retrograde transport between the Golgi apparatus and the endoplasmic reticulum (*20*, *21*).

Thus, the long-standing question of whether Arf1 and Arf1's GEF actually correlate to myelin sheath formation has been left unanswered. Here, we have generated conditional knockout mice for Arfgef1 [generally known as brefeldin A–inhibited guanine nucleotide-exchange protein 1 (BIG1)] and have investigated whether BIG1 is involved in the regulation of the initiation of myelination by Schwann cells. Compared with littermate controls, Schwann cell–specific BIG1 knockout mice result in decreased myelin thickness in sciatic nerves, especially in the initiation of myelination. The knockout mouse nerves exhibit a specific decrease in the amounts of Arf1 in an AP1 but not in those of Arf1 in a COPI. The binding of Arf1 to GGA1 is comparable in BIG1 knockout mice and controls. Furthermore, we have generated conditional Arf1 knockout mice, which have produced similar results in myelin thickness with BIG1 knockout mice. These results illustrate key roles for BIG1 and Arf1 in peripheral nerve system myelination, presenting previously unanticipated molecules involved in myelination.

[1]Laboratory of Molecular Neuroscience and Neurology, Tokyo University of Pharmacy and Life Sciences, Hachioji, Tokyo 192-0392, Japan. [2]Department of Pharmacology, National Research Institute for Child Health and Development, Setagaya, Tokyo 157-8535, Japan. [3]Department of Neuroscience, Baylor College of Medicine, Houston, TX 77030, USA. [4]Division of Structural Biochemistry, Jichi Medical University, Shimotsuke, Tochigi 329-0498, Japan. [5]Laboratory of Glycobiology, The Noguchi Institute, Itabashi, Tokyo 173-0003, Japan.
*These authors contributed equally to this work.
†Corresponding author. Email: yamauchi@toyaku.ac.jp

RESULTS

BIG1 is up-regulated during the peripheral nervous system development

To examine changes in expression of BIG1 and related molecules during development of the peripheral nervous system, we used mouse sciatic nerves and carried out immunoblotting with the respective specific antibodies. Expression levels of BIG1 increased until 7 days after birth. Elevated expression levels were very clearly detected until ~1 month, after which these levels decreased (fig. S1, A and B). BIG1 begins to up-regulate when myelination is initiated. On the other hand, levels of the BIG1 effector Arf1 and control proteins were comparable throughout the ages of mice used for immunoblotting. As mice developed, the expression levels of myelin protein zero (MPZ), the major peripheral myelin membrane protein, were increased.

BIG1 regulates the initiation of myelination in the peripheral nervous system

Thus, we investigated the effect of knockout of BIG1 in Schwann cells. We generated BIG1 conditional knockout mice that would be suitable for the Cre-loxP recombination system (Fig. 1A). Schwann cell–specific Dhh promoter–driven Cre recombinase transgenic mice were used for the deletion of loxP-flanked genes (*22*). Production of BIG1 conditional knockout (tentatively referred to as *BIG1*$^{fl/fl}$*; Dhh-Cre*) mice was confirmed by genomic polymerase chain reaction (PCR) and Southern blotting with specific primers and probes, respectively, using tail genomic DNA (Fig. 1, B and C). Through immunoblotting with the respective specific antibodies in sciatic nerves, BIG1 conditional knockout did not affect expression levels of Arf1 and actin, whereas it decreased MPZ levels (Fig. 1, D and E). The expression levels of Sox10 and Oct6 (also known as Scip or POU3F1), which are transcription factors controlling Schwann cell fate (*1*), were comparable in knockout mice and littermate controls (fig. S1, C and D). In contrast, the levels of Krox20 (also known as Egr2), which is a transcription factor required for triggering Schwann cell myelination (*1*), were decreased in knockout mice, revealing that BIG1 is involved in the regulation of myelination. As mice developed, the expression levels of Krox20, as well as those of MPZ, became comparable in knockout mice and controls (fig. S2, A and C), suggesting that BIG1 is involved in the regulation of myelination, especially for its initiation.

BIG1 plays a key role in controlling transporting systems in the Golgi network where Arf1 is activated. Arf1 participates in the assembly of AP1 subunit proteins, which are important for anterograde transports from the trans-Golgi (*16*–*18*). Also, Arf1 binds GGA1, which contributes primarily to transports from the trans-Golgi to the lysosome (*19*). To explore whether knockout of BIG1 has an effect on Arf1 interaction with these components, we prepared tissue lysates from the sciatic nerves of BIG1 conditional knockout (*BIG1*$^{fl/fl}$*; Dhh-Cre*) mice and littermate controls. A complex forming AP1 is composed of heterogeneous subunit proteins, including AP1B1, AP1G1, AP1M1, and AP1S1. Thus, we performed immunoprecipitation with an anti-AP1G1 antibody. In control experiments, Arf1 was co-immunoprecipitated with AP1G1. AP1B1, AP1M1, and AP1S1 were also contained in AP1G1 immunoprecipitates. In contrast, in knockout mouse tissue lysates, the amounts of Arf1, as well as those of AP1B1, AP1M1, and AP1S1 in AP1G1 immunoprecipitates, were greatly decreased (Fig. 1, F and G), indicating the involvement of BIG1 in AP1 formation. Expression levels of Arf1, AP1B1, AP1G1, AP1M1, and AP1S1 were comparable in knockout mice and controls. Similarly, we performed immunoprecipitation with an anti-GGA1 antibody. The amounts of Arf1 in GGA1 immunoprecipitates were comparable in knockout mouse and control tissue lysates (fig. S3, A and B), and expression levels of Arf1 and GGA1 were also comparable.

In addition, Arf1 is important for the assembly of subunit proteins forming COPI, which participates in retrograde transports from the trans-Golgi to the endoplasmic reticulum (*20*, *21*). Immunoprecipitation with an antibody for COPB1, whose subunit constitutes a COPI's first subcomponent group with other subunit proteins COPD, COPG1, and COPZ1, was comparable in knockout mouse and control tissue lysates (fig. S3, C and D). Expression levels of Arf1, COPB1, COPD, COPG1, and COPZ1 were also comparable. Collectively, BIG1 primarily regulates the AP1 transporting system in Schwann cells.

Because BIG1 conditional knockout mice exhibited decreased MPZ and Krox20 levels, we analyzed the myelin sheath ultrastructure in sciatic nerves. Electron microscopic analysis revealed decreased myelin thickness in sciatic nerves from 7-day-old knockout (*BIG1*$^{fl/fl}$*; Dhh-Cre*) mice, compared to those from controls (Fig. 2A). This decreased myelin thickness in knockout mice is clearly evident from the quantification of the average *g*-ratio, which is the numerical average ratio of the axon diameter to the diameter of the outermost myelinated fiber. Thinner myelin sheaths with larger average *g*-ratios were generated in 5-day-old knockout mice (0.94 ± 0.035 in knockout mice, compared to 0.76 ± 0.061 in controls; Fig. 2, B and C). Similar results (Fig. 2D) were observed in 2-month-old knockout mice (0.70 ± 0.049 in knockout mice, compared to 0.63 ± 0.036 in controls; Fig. 2, E and F), revealing that the reduction in myelin thickness persists throughout development in knockout mice. Although the difference of average *g*-ratios between knockout mice and controls was significant, it became smaller as development proceeded. Therefore, these findings suggest that BIG1 is required for myelination, especially for its initiation. High-magnification electron microscopic analysis indicated that decreased myelin thickness was not due to a difference of thickness between the myelin sheath and the neighboring myelin sheath but was due instead to decreased numbers of wrapping myelin membranes (fig. S4A).

To confirm that these results are not specific to Dhh promoter–driven Cre recombinase–mediated conditional knockout, we also crossbred other Schwann cell–specific, MPZ promoter–driven Cre recombinase transgenic mice (*23*) with BIG1 floxed mice and generated conditional knockout (referred to as *BIG1*$^{fl/fl}$*; MPZ-Cre*) mice. Consistent with the results from *BIG1*$^{fl/fl}$*; Dhh-Cre* mice, thinner myelin sheaths, along with decreased MPZ expression, were also observed in knockout mice (0.83 ± 0.049 in knockout mice, compared to 0.70 ± 0.055 in controls; fig. S5) at 7 days postnatal.

BIG1 knockout does not affect cell proliferation or apoptosis

To investigate whether thin myelin sheaths observed in *BIG1*$^{fl/fl}$*; Dhh-Cre* mice are associated with cell proliferation and apoptosis, we stained 7-day-old sciatic nerves with antibodies for cell proliferation antigen Ki67 and active caspase-3 cleaved at the Asn^{175} position. Staining for Ki67 (fig. S6, A and B) and cleaved caspase-3 (fig. S7, A and B) was comparable in knockout mice and controls. The cross sections of sciatic nerves contain cell bodies of Schwann cells but not those of neuronal cells. Similar results were obtained from immunoblotting in developing sciatic nerves (figs. S6C and S7C). Knockout of BIG1 does not have obvious effects on Schwann cell proliferation and apoptosis.

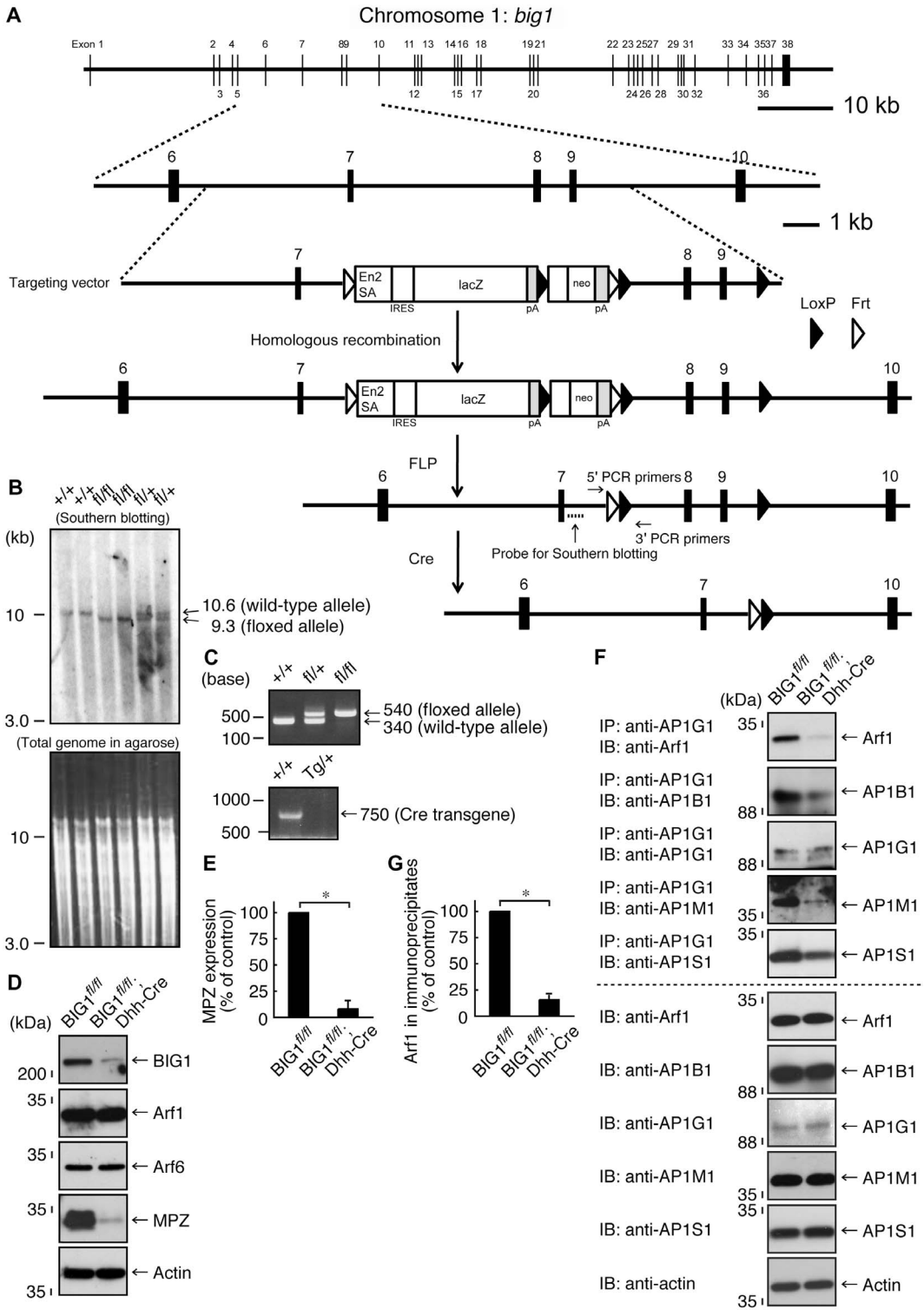

Fig. 1. Dhh-Cre–mediated BIG1 knockout mice are generated, exhibiting a decreased amount of Arf1 in AP1 adaptor protein subunits and a decreased MPZ expression. (**A**) Schwann cell–specific (in this case, Dhh promoter–controlled) Cre recombinase transgenic mice were used for deletion of the loxP-flanked exons of the *big1* gene. The knockout cassette, as well as the primer and probe positions, is shown. (**B**) The loxP-flanked exons, which were digested by Spe I and Sac I, were confirmed with Southern blotting using a specific probe. (**C**) Genetically modified mice (floxed and Cre mice) were identified with the tail's genomic PCR using the respective, specific primers. (**D** and **E**) Sciatic nerve tissue lysates of conditional knockout (*BIG1*$^{fl/fl}$; *Dhh-Cre*) mice and their littermate controls were used for immunoblotting with the respective antibodies for BIG1, Arf1, Arf6, MPZ, and control actin. MPZ expression levels are statistically shown (*$P < 0.01$; $n = 3$ blots). (**F** and **G**) Tissue lysates were used for immunoblotting with the respective antibodies for Arf1, AP1B1, AP1G1, AP1M1, and AP1S1, following immunoprecipitation with an anti-AP1G1 antibody. Total proteins and Arf1 co-immunoprecipitation's statistical data (*$P < 0.01$; $n = 3$ blots) are also shown.

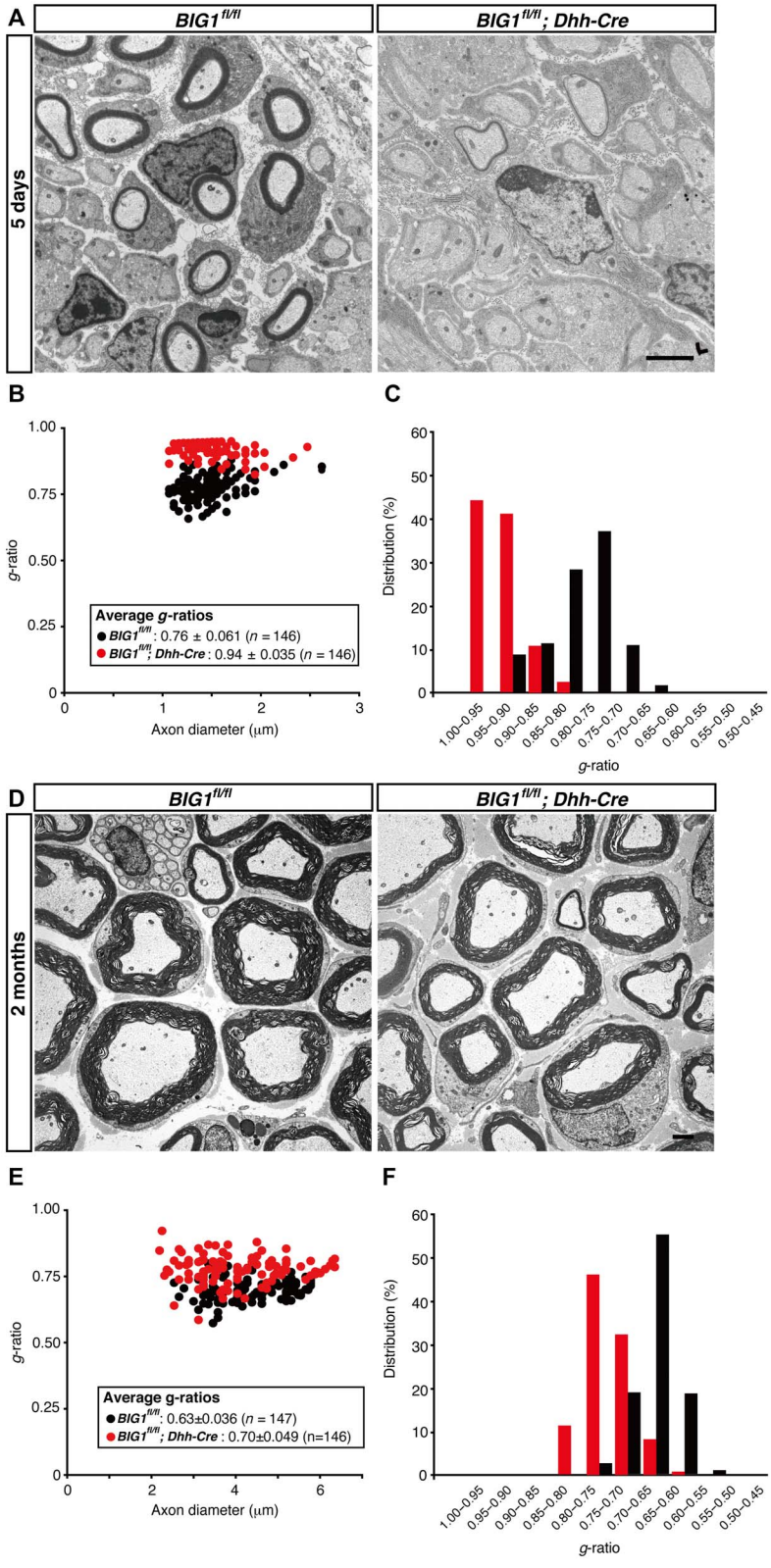

Fig. 2. Dhh-Cre–mediated BIG1 knockout mice exhibit decreased myelin thickness. (**A**) Electron microscopic images of sciatic nerve cross sections of conditional knockout (*BIG1*$^{fl/fl}$*; Dhh-Cre*) and control mice at 5 days postnatal are shown. Scale bar, 1 μm. (**B** and **C**) A graph of *g*-ratios of myelinated axons for axon diameters, as well as their distributions, is shown (*n* = 146 nerves for knockout mice and *n* = 146 nerves for controls; three independent mice). (**D**) Electron microscopic images of sciatic nerve cross sections of conditional knockout and control mice at 2 months postnatal are shown. Scale bar, 1 μm. (**E** and **F**) A graph of *g*-ratios of myelinated axons for axon diameter, as well as their distributions, is shown (*n* = 146 nerves for knockout mice and *n* = 147 nerves for controls; three independent mice).

Arf1 regulates the initiation of myelination in the peripheral nervous system

Next, we asked whether Arf1 is involved in the regulation of myelination by Schwann cells. We generated Arf1 conditional knockout (tentatively referred to as *Arf1*$^{fl/fl}$; *Dhh-Cre*) mice (Fig. 3A). The mice were confirmed by genomic PCR and Southern blotting (Fig. 3, B and C). Although Arf1 conditional knockout mice did not affect expression levels of BIG1 and actin, they did exhibit decreased MPZ levels (Fig. 3, D and E). The expression levels of Sox10 and Oct6 were comparable in knockout mice and controls (fig. S1, E and F); in contrast, those of Krox20 were decreased in knockout mice, revealing that Arf1 is involved in the regulation of myelination. As mice developed, the expression levels of Krox20, as well as those of MPZ, became comparable in knockout mice and controls (fig. S2, B and D), suggesting that Arf1 is involved in the regulation of myelination, especially for its initiation.

In electron microscopic analysis, 7-day-old knockout (*Arf1*$^{fl/fl}$; *Dhh-Cre*) mice exhibited decreased myelin thickness, compared to those from controls (Fig. 4A). This decreased myelin thickness in conditional knockout mice is clearly evident from quantification of the average *g*-ratio (0.82 ± 0.060 in knockout mice, compared to 0.72 ± 0.036 in the controls; Fig. 4, B and C). Similar results (Fig. 4D) were observed in 2-month-old knockout mice (0.68 ± 0.047 in knockout mice, compared to 0.65 ± 0.033 in controls; Fig. 4, E and F). These results reveal the reduction in myelin thickness throughout development in knockout mice, although the difference of average *g*-ratios between knockout mice and controls decreased as development proceeded. It is suggested that Arf1 is required for the initiation of myelination. High-magnification electron microscopic analysis indicated that the thickness between the myelin sheath and the neighboring myelin sheath was comparable in knockout mice and controls (fig. S4B).

We also crossbred MPZ promoter–driven Cre recombinase transgenic mice with Arf1 floxed mice to generate conditional knockout (referred to as *Arf1*$^{fl/fl}$; *MPZ-Cre*) mice. Consistent with the results from *Arf1*$^{fl/fl}$; *Dhh-Cre* mice, thinner myelin sheaths, along with decreased

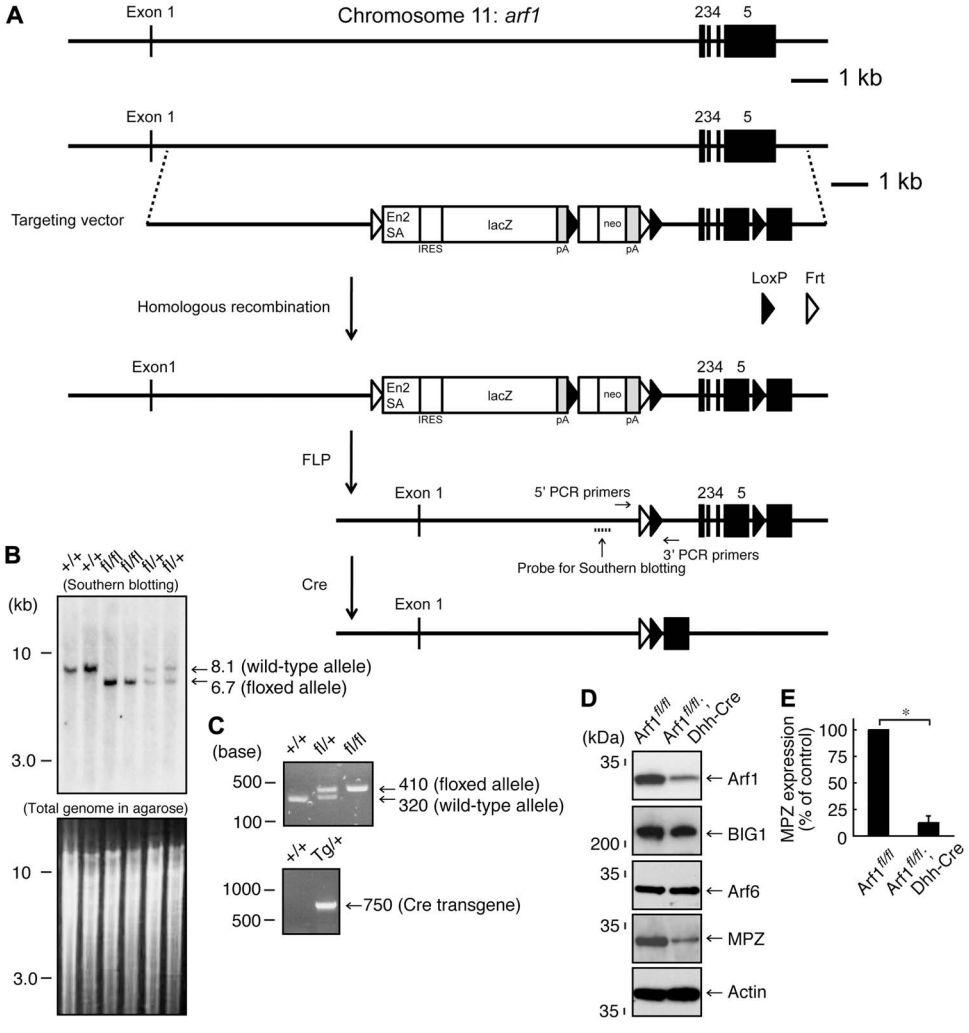

Fig. 3. Dhh-Cre–mediated Arf1 knockout mice are generated, exhibiting a decreased MPZ expression. (**A**) Schwann cell–specific (in this case, Dhh promoter–controlled) Cre recombinase transgenic mice were used for deletion of the loxP-flanked exons of the *arf1* gene. The knockout cassette, as well as the primer and probe positions, is shown. (**B**) The loxP-flanked exons, which were digested by Eco RV, were confirmed with Southern blotting using specific probes. (**C**) Genetically modified mice (floxed and Cre mice) were identified with the tail's genomic PCR using the respective, specific primers. (**D** and **E**) Sciatic nerve tissue lysates of conditional knockout (*Arf1*$^{fl/fl}$; *Dhh-Cre*) mice and their littermate controls were used for immunoblotting with the respective antibodies for BIG1, Arf1, Arf6, MPZ, and control actin. MPZ expression levels are statistically shown (*P < 0.01; n = 3 blots).

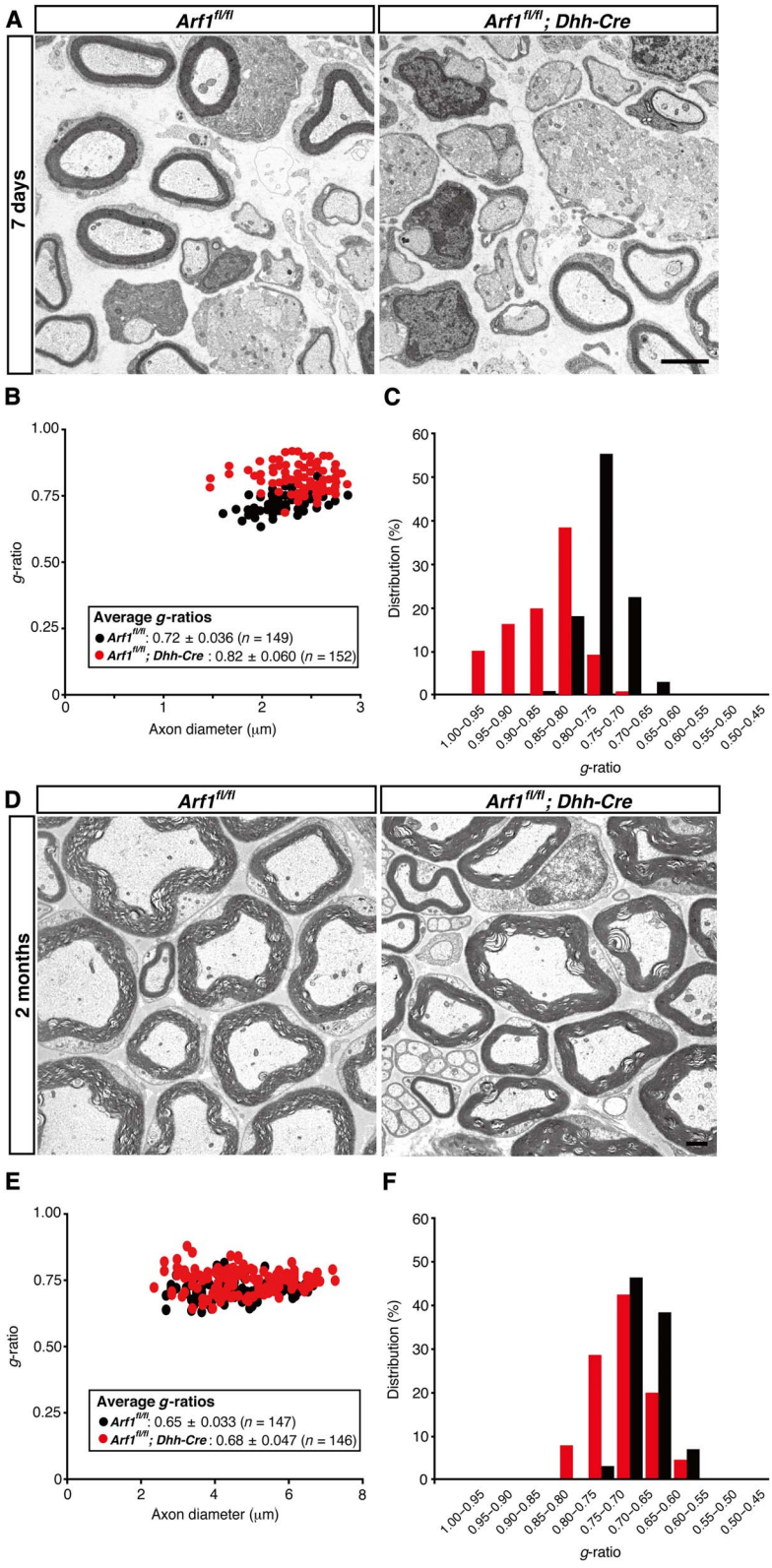

Fig. 4. Dhh-Cre–mediated Arf1 knockout mice exhibit decreased myelin thickness. (**A**) Electron microscopic images of sciatic nerve cross sections of conditional knockout (*Arf1*$^{fl/fl}$*; Dhh-Cre*) and control mice at 7 days postnatal are shown. Scale bar, 1 μm. (**B** and **C**) A graph of *g*-ratios of myelinated axons for axon diameters, as well as their distributions, is shown (n = 152 nerves for knockout mice and n = 149 nerves for controls; three independent mice). (**D**) Electron microscopic images of sciatic nerve cross sections of conditional knockout and control mice at 2 months postnatal are shown. Scale bar, 1 μm. (**E** and **F**) A graph of *g*-ratios of myelinated axons for axon diameters, as well as their distributions, is shown (n = 146 nerves for knockout mice and n = 147 nerves for controls; three independent mice).

MPZ expression, were observed in knockout mice (0.78 ± 0.047 in knockout mice, compared to 0.71 ± 0.059 in controls; fig. S8) at 7 days postnatal.

Arf1 knockout does not affect cell proliferation or apoptosis

We stained 7-day-old Arf1 conditional knockout mouse (*Arf1*$^{fl/fl}$; *Dhh-Cre*) sciatic nerves with antibodies for Ki67 and active, cleaved caspase-3. Staining for Ki67 (fig. S9, A and B) and cleaved caspase-3 (fig. S10, A and B) indicated comparable results in knockout mice and controls. Similar results were obtained from immunoblotting in developing sciatic nerves (figs. S9C and S10C).

Knockout of BIG1 or Arf1 decreases MPZ distribution in growing myelin sheaths

Since BIG1 conditional knockout mice exhibited decreased amounts of Arf1 in active AP1 subunits, with a thin myelin thickness phenotype, we asked whether knockout of BIG1 or Arf1 is actually associated with a defect of the intracellular transporting system. Myelin components are transported from cell bodies of Schwann cells via various systems, one of which may be the AP1 transporting system (*24*–*26*). Multiple myelin layers are formed by incorporating newly generated, growing myelin membranes underneath previously completed membranes (*27*). Therefore, if there is a defect of the transporting system in the case of either protein or mRNA level, there are relatively smaller amounts of the myelin component in the inner myelin sheaths. Thus, we tried to detect an MPZ antigen of myelin sheaths by immune electron microscopy (*28*). MPZ is a myelin component, and it contributes to the interaction of the myelin sheath with the neighboring myelin sheath. BIG1 knockout mice (*BIG1*$^{fl/fl}$; *Dhh-Cre*) showed a decrease in the relative amounts of MPZ in inner myelin sheaths (Fig. 5, A and B). Similar results are obtained from Arf1 knockout mice (*Arf1*$^{fl/fl}$; *Dhh-Cre*; Fig. 5, C and D), suggesting that BIG1 and Arf1 constitute one of the transporting systems of the myelin component. It is likely that BIG1 and Arf1 are involved in the regulation of myelin formation through the transporting of a myelin component. Also, uneven MPZ distribution in knockout mice may be due to delayed induction of MPZ expression during development (fig. S2).

DISCUSSION

In the peripheral nervous system, myelin sheaths result in the Schwann cell plasma membranes forming multiple layers. The total area of the sheaths often grows to more than 100 times larger than that of the plasma membranes of premyelinating Schwann cells. Thus, myelination processes undergo continuous and dynamic morphological changes, which involve not only cytoskeletal rearrangements but also various types of transport (*3*–*5*). These two cellular events are generally linked to cell morphological changes and, in turn, tissue morphogenesis in many types of cells and tissues where Arf proteins contribute, at least in part, to their morphogenesis (*6*–*9*). The question of whether the prototypic Arf family protein Arf1 actually regulates formation of multiple myelin sheaths remains unanswered. Here, we show that Arf1 GEF, BIG1, and the effector Arf1 are required for the initiation of myelination in the peripheral nervous system. The conclusions are obtained from the data using generated BIG1 and Arf1 conditional knockout mice. Compared to littermate controls, decreased myelin thickness is observed in Schwann cell–specific BIG1 conditional knockout mice, especially in the initiation of myelination. The amounts of Arf1 in AP1 subunits are greatly decreased in knockout mice. In contrast, the amounts of Arf1 in COPI subunits and Arf1 binding to GGA1 are comparable in BIG1 knockout mice and controls, revealing that BIG1 primarily regulates the AP1 transporting system in Schwann cells. Decreased myelin thickness is also observed in Schwann cell–specific Arf1 conditional knockout mice. Thus, BIG1 and Arf1 contribute to the initiation of myelination in the peripheral nervous system. This proposal is further supported by the results showing that expression levels of the myelination-related transcription factor Krox20, as well as those of the major myelin membrane protein MPZ, become comparable in BIG1 or Arf1 knockout mice and controls as mice develop. Furthermore, since it is unlikely that BIG1 and Arf1 are directly involved in the regulation of the transcription factor (*7*–*9*), they may mediate Krox20 expression through activities of signaling molecules directly controlling expression of the transcription factor in early developmental stages. Further studies will allow us to clarify whether or how BIG1 and Arf1, acting together with identified or unidentified interacting molecules, promote myelination, probably by mediating the transportation of myelin components and the expression of identified and unidentified myelination-related transcription factors.

Thus far, genomes of human and rodents as the model encode ~15 GEFs for Arf proteins, whose common feature is to contain catalytic Sec7 domains (*6*–*9*). Among them, GEFs harboring catalytic activity for Arf6 include more than 10 molecular species. We previously reported the involvement of cytohesin subfamily GEFs as the Arf6 GEF involved in myelination by Schwann cells (*12*, *29*, *30*). When myelination is initiated, cytohesin-1 is expressed at high levels. Cytohesin-1 probably supports the activity of Arf6 in Schwann cells in initiating myelination. Following development, cytohesin-2, rather than cytohesin-1, is up-regulated to stimulate the Arf6 activity. It is likely that cytohein-2 is required for sustaining myelination. Despite the participation of Arf6 GEFs and cytohesin-1 and cytohesin-2 in myelination, it remains unclear whether a GEF for Arf1 is involved in the regulation of myelination. GEFs for Arf1 are composed of two distinct families: BIG1 and its homologs and Golgi brefeldin A resistance factor 1 (GBF1) (*17*, *18*, *20*, *21*). BIG1 generally functions as the GEF of Arf1 on the trans-Golgi and mediates anterograde transports in the trans-Golgi network where an AP1 complex functions. On the other hand, GBF1 functions as the Arf1 GEF on the cis-Golgi to control retrograde transports in the direction from the Golgi apparatus to the endoplasmic reticulum where a COPI complex functions. Myelin formation in early, postnatal developmental stages requires very active transport throughout the trans-Golgi network to the peripheral regions of the myelin membrane (*25*). Furthermore, it is possible that BIG2, a molecule closely related to BIG1, regulates myelination. Transcriptional products of BIG1 are broadly detected throughout various tissues including nerve tissues, whereas those of BIG2 are detected at a relatively low level (see the UniGene website, www.ncbi.nlm.nih.gov/unigene/). Additional studies on the distribution of BIG1 and BIG2 transcriptional products will shed light on their roles, although BIG1 is involved in initiating myelination in the peripheral nervous system. Acting with other GEF(s) for Arf1 and Arf proteins, BIG1 may play key roles in myelination.

Although the molecular mechanism by which GEFs are activated is complicated and varied depending on the GEF subfamilies involved, phosphorylation events of GEFs themselves are well recognized as one of the major regulatory factors. The phosphorylating mechanism involved in the activation of Vav, which is the GEF specific for the Rho family GTPase RhoA, has been previously identified (*31*). Vav has an autoinhibitory domain for catalytic domain, and the region is released upon Vav's tyrosine phosphorylation. The catalytic domain

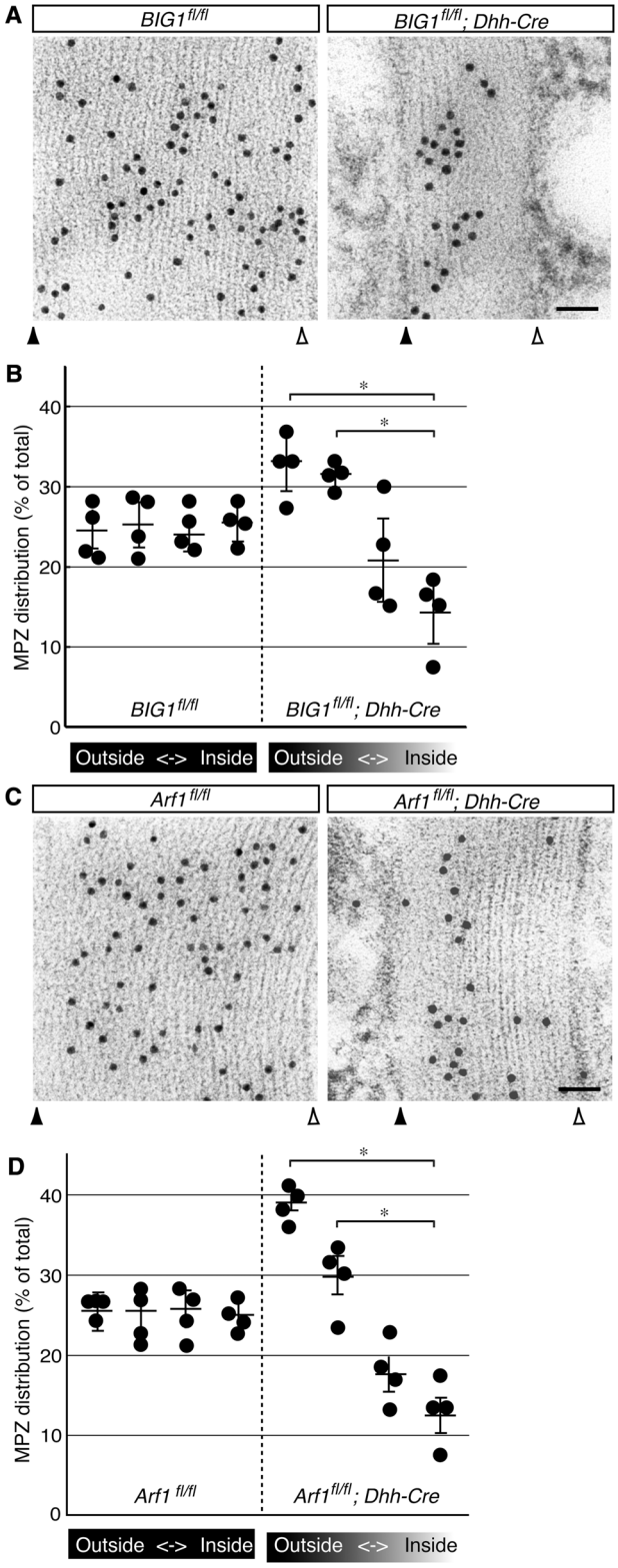

Fig. 5. Dhh-Cre–mediated BIG1 or Arf1 knockout mice decrease MPZ localization in inner myelin sheaths. (**A**) Sciatic nerve images of conditional knockout (*BIG1$^{fl/fl}$; Dhh-Cre*) and control mice at 7 days postnatal are shown. MPZ antigens (black dots in images) in nerve cross sections were observed with immunoelectron microscopy. Closed and open triangles indicate outside and inside positions of myelin sheaths. Scale bar, 50 nm. (**B**) The statistical data for MPZ distribution at every 25% intervals from the outer to inner myelin sheaths are shown in the graph (*$P < 0.01$; $n = 3$ independent mice). (**C**) Similarly, sciatic nerve images of conditional knockout (*Arf1$^{fl/fl}$; Dhh-Cre*) and control mice at 7 days postnatal are shown. Closed and open triangles indicate outside and inside positions of myelin sheaths. Scale bar, 50 nm. A nonspecific binding particle in knockout and control mice is seen in the outside of the myelin sheaths. (**D**) Statistical data are shown in the graph (*$P < 0.01$; $n = 3$ independent mice).

of Vav results in the interaction with RhoA to be activated. A similar mechanism is also conserved in the case of the activation of cytohesin-1 (*12*). Tyrosine phosphorylation of an autoinhibitory region in cytohesin-1 releases its region from the catalytic domain. In turn, Arf6 interacts with the catalytic domain of cytohesin-1. BIG1 has many potential phosphorylation sites involving tyrosine and serine/threonine kinases (see the NetPhos website, www.cbs.dtu.dk/services/NetPhos/). The activity of BIG1 may be regulated by phosphorylation.

Hereditary peripheral neuropathies are associated with GEFs for Rho family GTPases. The mutation of the *arhgef10* (also known as *gef10*) gene is responsible for a peripheral neuropathy with thinly myelinated axons (*32*). The gene product is a GEF specific for RhoA. The mutation results in slowed nerve conduction velocities, as seen in Charcot-Marie-Tooth (CMT) diseases. Also, the mutation of the *frabin* [also called *fyve*, *rho-gef*, and *pleckstrin homology domain containing 4* (*fgd4*)] gene causes CMT disease type 4H (*33*, *34*). Frabin is a GEF specific for Cdc42. The mutations of the *arhgef10* and *frabin* are probably associated with improper regulation of their gene products and affect Schwann cell morphological changes. On the other hand, the mutation of the *big2* (also known as *arfgef2*) gene is linked to periventricular heterotopia with microcephaly, which involves a severe developmental defect of the cerebral cortex in the central nervous system (*35*). Because BIG1, as well as BIG2, plays multiple roles involving cell morphological changes (*8*, *9*), it could be noteworthy to investigate the association of the *big1* gene with peripheral and central neuropathies.

Here, we identify BIG1 and Arf1 as the regulatory molecules of myelination in the peripheral nervous system. Further studies will enhance our understanding not only of how BIG1 and Arf1 are regulated in a series of myelination processes but also of the detailed mechanism by which they physically and physiologically associate with their upstream or downstream molecules during myelination. Along this line, such studies on the relationship of the BIG1 and Arf1 unit with myelination may provide us with a paradigm of the molecular basis for remyelination and nerve regeneration.

MATERIALS AND METHODS

Antibodies

The following antibodies were purchased: rabbit polyclonal anti-AP1G1 [cat. no. ab21980; immunoblotting (IB), 1/1000; immunoprecipitation (IP), 1 μg per lysate], rabbit monoclonal anti–caspase-3 (cat. no. ab32351; IB, 1/5000), rabbit monoclonal anti-Krox20 (cat. no. ab108399; IB, 1/5000), rabbit monoclonal anti-Oct6 (cat. no. ab126746; IB, 1/5000), and rabbit monoclonal anti-Sox10 (cat. no. ab155279; IB, 1/5000) from Abcam; mouse polyclonal anti-AP1M1 (cat. no. H00008907-A1; IB, 1/500) from Abnova; rabbit polyclonal anti-Ki67 [proliferating cell marker, cat. no. 9129; immunofluorescence (IF), 1/500] and rabbit polyclonal anti-cleaved caspase-3 (apoptotic cell marker, cat. no. 9661; IF, 1/500) from Cell Signaling Technology; rabbit polyclonal anti-BIG1 (cat. no. HPA023822; IB, 1/100) from Atlas Antibodies; mouse monoclonal anti-actin β type (cat. no. M177-3; IB, 1/5000) and rabbit polyclonal anti-MPZ (cat. no. PD046; IB, 1/250; immunoelectron microscopy, 1/2500) from MBL; rabbit polyclonal anti-AP1S1 (cat. no. TA331243; IB, 1/500) from Origene; and mouse monoclonal anti-Arf1 (cat. no. sc-53168; IB, 1/50), mouse monoclonal anti-Arf6 (cat. no. sc-7971; IB, 1/25), rabbit polyclonal anti-AP1B1 (cat. no. sc-10762; IB, 1/100), mouse monoclonal anti-COPB1/COPB (cat. no. sc-393615; IB, 1/100; IP, 1 μg per lysate), mouse monoclonal anti-COPD (cat. no. sc-514104; IB, 1/25), mouse monoclonal anti-COPG1/COPG (cat. no. sc-393977; IB, 1/100), mouse monoclonal anti-COPZ1/COPZ (cat. no. sc-398219; IB, 1/100), mouse monoclonal anti-GGA1 (cat. no. sc-390837; IB, 1/50; IP, 1 μg per lysate), and goat polyclonal anti-Sox10 (Schwann cell lineage cell marker, cat. no. sc-17342; IF, 1/50) from Santa Cruz Biotechnology. The standard secondary antibodies (peroxidase-conjugated and fluorescent substance–labeled antibodies) were purchased from MBL or Thermo Fisher Scientific.

Generation and propagation of genetically modified mice

EuMMCR BIG1 conditional knockout C57BL/6 mouse ES [Arfgef1tm1a (EUCOMM)Hmgu] cells were purchased from Eucomm to generate chimeric mice. First, to identify the neo gene-containing knockout cassette, offspring were genotyped by genomic PCR. To evaluate the knockout cassette allele, the primers used were 5′-CTTCCTCGTGCTTTACGGTATC-3′ (sense) and 5′-ATGTAGAACATACCTCAATTTGCATC-3′ (antisense) for the knockout cassette long arm position and 5′-GTTCTTTTTGTCCTGTGGAATCTTA-3′ (sense) and 5′-TGCACATCCTTTCTCAAATAGTGTA-3′ (antisense) for the knockout cassette short arm position. In the former primer pair, the allele harboring knockout cassette displayed ~6700 base pairs (bp). In the later primer pair, the allele harboring knockout cassette displayed ~530 bp, enabling us to obtain 11 chimeric mice. Next, to remove the neo gene, offspring were mated with Unitech Flp recombinase transgenic mice (Unitech). To evaluate the neo gene deletion allele, the primers used were 5′-TAGTTAAGAATGTTCCCACATGTCC-3′ (sense) and 5′-ACATGGTCTATAAGTTGCAGTAGCA-3′ (antisense) for the long arm position and 5′-GAACAAGATGGATTGCACGCAGGTTCTCCG-3′ (sense) and 5′-GTAGCCAACGCTATGTCCTGATAG-3′ (antisense) for the neo gene. In the former primer pair, the knockout allele with the neo gene, the knockout allele without the neo gene (also called the floxed allele), and the wild-type allele displayed ~7400, ~540, and ~340 bp, respectively. In the later primer pair, the allele with the neo gene displayed ~670 bp, enabling us to obtain 10 hemizygotic floxed knockout mice. Finally, to remove the flp gene, these mice were further mated with the wild-type C57BL/6 mice (Sankyo Inc.). The primers used were 5′-TAGTTTGCAATTACAGTTCGAATCA-3′ (sense) and 5′-AGCCTTGTTGTACGATCTGACTAAG-3′ (antisense) for the flp gene.

The primers used for BIG1 conditional knockout mouse genotyping were 5′-TAGTTAAGAATGTTCCCACATGTCC-3′ (sense) and 5′-ACATGGTCTATAAGTTGCAGTAGCA-3′ (antisense). The floxed and the wild-type alleles displayed ~540 and ~340 bp, respectively. Southern blotting, using 504 bp between exons 7 and 8 of the gene encoding BIG1 as the specific probe, confirmed that the floxed and the wild-type alleles were ~9.3 and ~10.6 kbp, respectively.

Also, EuMMCR Arf1 conditional knockout C57BL/6 mouse ES [Arf1tm1a(EUCOMM)Wtsi] cells were obtained from Eucomm to generate chimeric mice. First, to evaluate the knockout cassette allele of the offspring, the primers used were 5′-CTTCCTCGTGCTTTACGGTATC-3′ (sense) and 5′-ATCCCGAGTATGATCTTGTTCTGAG-3′ (antisense) for the knockout cassette long arm position and 5′-AATGCTAGATATCAGATCACCTGTT-3′ (sense) and 5′-ATGCAGCGGATGGTGGTTTGTTCATC-3′ (antisense) for the knockout cassette short arm position. In the former primer pair, the allele harboring knockout cassette displayed ~7100 bp. In the later primer pair, the allele harboring knockout cassette displayed ~160 bp, enabling us to obtain six chimeric mice. Next, to remove the neo gene, the primers used were 5′-GTTGAAAATTGTGGATACTTTGACAC-3′

(sense) and 5′-TGAAGGGACATCTAACTACAATCAA-3′ (antisense) for the long arm position and 5′-GAACAAGATGGATTGCACG-CAGGTTCTCCG-3′ (sense) and 5′-GTAGCCAACGCTATGTCCT-GATAG-3′ (antisense) for the neo gene. In the former primer pair, the knockout allele with the neo gene, the knockout allele without the neo gene, and the wild-type allele displayed ~7300, ~410, and ~320 bp, respectively. In the later primer pair, the allele with the neo gene displayed ~670 bp, enabling us to obtain four hemizygotic floxed knockout mice. Finally, to remove the flp gene, these mice were further mated with the wild-type C57BL/6 mice.

The primers used for Arf1 conditional knockout mouse genotyping were 5′-GTTGAAAATTGTGGATACTTTGACAC-3′ (sense) and 5′-TGAAGGGACATCTAACTACAATCAA-3′ (antisense). The floxed and the wild-type alleles displayed ~410 and ~320 bp, respectively. Southern blotting, using 307 bp between exons 1 and 2 of the gene encoding Arf1 as the specific probe, confirmed that the floxed and the wild-type alleles were ~6.7 and ~8.1 kbp, respectively.

To delete the gene specifically in Schwann cells, BIG1 or Arf1 conditional knockout mice were mated with Dhh or MPZ promoter–controlled Cre recombinase transgenic mice (stock no. 012929 or 017927, The Jackson Laboratory). The PCR primers used to identify the *cre* transgene were 5′-TTTGCCTGCATTACCGGTCGATG-CAAC-3′ (sense) and 5′-GCGCGAGTTGATAGCTGGCTGGTG-3′ (antisense). The product was ~750 bp.

In all experiments, PCR amplification (using LA or EX Taq polymerase; Takara Bio) was performed in 35 cycles, with each cycle consisting of denaturation at 94°C for 1 min, annealing at 60° to 68°C for 1 min, depending on the primer pair's annealing temperature, and extension at 72°C for 1 or 5 min.

When it was possible to determine their sex, male mice were used for experiments. Homozygous mice, as well as heterozygous mice, were fertile under standard breeding conditions.

Tissue lysis, immunoprecipitation, and immunoblotting

Tissues were lysed in lysis buffer A [50 mM Hepes-NaOH (pH 7.5), 3 mM $MgCl_2$, 150 mM NaCl, 1 mM dithiothreitol, 1 mM phenylmethane sulfonylfluoride, leupeptin (1 μg/ml), 1 mM EDTA, 1 mM Na_3VO_4, and 10 mM NaF] containing biochemical detergents (0.5% NP-40, 1% CHAPS, and 0.03% SDS). Unless otherwise indicated, all lysis steps were performed at 4°C (*12*, *36*). For immunoprecipitations, the supernatants cleared by centrifugation were mixed with an antibody-absorbed protein G resin (GE Healthcare) or ExtraCruz (Santa Cruz Biotechnology) according to the respective manufacturer's instructions. The immunoprecipitates or proteins in the cell supernatants were denatured, subjected to SDS–polyacrylamide gel electrophoresis, and blotted to polyvinylidene difluoride membranes using the TransBlot TurboTransfer System (Bio-Rad). The membranes were blocked with Blocking One (Nacalai) and immunoblotted using a primary antibody followed by a peroxidase-conjugated secondary antibody. The bound antibodies were detected using Chemiluminescence One (standard and strong detection reagents; Nacalai). The bands were scanned using a C-DiGit Blot Scanner (MS Systems). They were densitometrically analyzed to identify their quantification using UN-SCAN-IT software (Silk Scientific).

Tissue immunofluorescence

Nerve tissues were perfused with phosphate-buffered saline (PBS) and then with PBS containing 4% paraformaldehyde (*12*, *36*). They were postfixed with 4% paraformaldehyde, replaced with 20% sucrose, and embedded in a Tissue-Tek reagent (Sakura Finetechnical). Microtome sections (NX70; Thermo Fisher Scientific) were blocked with Blocking One and incubated first with a primary antibody and then with a fluorescent substance–labeled secondary antibody. The glass coverslips were mounted with Vectashield Mounting Medium (Vector Laboratories). The fluorescent images were collected with an IX81 microscope system with a laser-scanning FV500 or FV1000D (Olympus). Fluorescent substance–labeled cells were considered to be those with a value greater than 5000 using UN-SCAN-IT software.

Electron microscopy and immunoelectron microscopy

For electron microscopy (*12*, *36*), nerve tissues were fixed with 2% paraformaldehyde and 2% glutaraldehyde in 0.1% cacodylate buffer, contrasted with 2% osmium tetroxide, dehydrated with an ethanol gradient, and treated with propylene oxide. Finally, samples were infiltrated and embedded in pure epoxy. Ultrathin sections (Ultracut UCT; Leica) were stained with uranyl acetate and lead staining solution.

For immunoelectron microscopy (*28*), tissues were fixed with 4% paraformaldehyde and 0.1% glutaraldehyde in PBS, dehydrated with an ethanol gradient, and infiltrated with a 1:1 mixture of ethanol and resin (LR white; London Resin). The samples were transferred to 100% resin and polymerized by an ultraviolet polymerizer. Ultrathin sections were mounted with nickel grids. Grids were blocked, incubated first with a primary antibody and then with a 10-nm-diameter gold particle–conjugated secondary antibody. They were then stained with uranyl acetate and lead staining solution. Images were taken with a JEM-1200EX or JEM-1400 Plus electron microscope system (JEOL). The *g*-ratio is the ratio of axon diameters to the outer myelinated axon diameters. These ratios were plotted for axon diameter. Their distributions were also shown in the graph.

Statistical analysis

Values are means ± SD from separate experiments. Intergroup comparisons were performed by Student's *t* test using Microsoft Excel. A one-way analysis of variance (ANOVA) was followed by a Fisher's protected least significant difference test as a post hoc comparison using AnalystSoft StatPlus. Differences were considered significant when $P < 0.05$.

Ethics statement

Genetically modified/unmodified rodents were generated and maintained in accordance with a protocol approved both by the Tokyo University of Pharmacy and Life Sciences Animal Care Committee and by the Japanese National Research Institute for Child Health and Development Animal Care Committee.

SUPPLEMENTARY MATERIALS

Supplementary material for this article is available at http://advances.sciencemag.org/cgi/content/full/4/4/eaar4471/DC1

fig. S1. Changes in expression levels of BIG1, the related proteins, and myelin marker protein MPZ during sciatic nerve development and the effect of BIG1 or Arf1 knockout on myelination-related transcription factor Krox20 expression.
fig. S2. Effects of knockout of BIG1 or Arf1 on Krox20 or MPZ expression during development.
fig. S3. Effects of knockout of BIG1 on the amounts of Arf1 in transporting protein complexes.
fig. S4. Comparison of thickness between the myelin sheath and the neighboring myelin sheath in Dhh-Cre–mediated BIG1 or Arf1 knockout mice and controls.
fig. S5. MPZ-Cre–mediated BIG1 knockout mice exhibit decreased myelin thickness.
fig. S6. Staining for the proliferating cell marker (Ki67) in Dhh-Cre–mediated BIG1 knockout and control mouse nerve cross sections and Ki67 expression during development.
fig. S7. Staining for the apoptotic cell marker (cleaved caspase-3) in Dhh-Cre–mediated BIG1 knockout and control mouse nerve cross sections and caspase-3 expression during development.

fig. S8. MPZ-Cre–mediated Arf1 knockout mice exhibit decreased myelin thickness.
fig. S9. Staining for the proliferating cell marker (Ki67) in Dhh-Cre–mediated Arf1 knockout and control mouse nerve cross sections and Ki67 expression during development.
fig. S10. Staining for the apoptotic cell marker (cleaved caspase-3) in Dhh-Cre–mediated Arf1 knockout and control mouse nerve cross sections and caspase-3 expression during development.

REFERENCES AND NOTES

1. R. Mirsky, K. R. Jessen, Schwann cell development, differentiation and myelination. *Curr. Opin. Neurobiol.* **6**, 89–96 (1996).
2. K.-A. Nave, J. L. Salzer, Axonal regulation of myelination by neuregulin 1. *Curr. Opin. Neurobiol.* **16**, 492–500 (2006).
3. C. Taveggia, M. L. Feltri, L. Wrabetz, Signals to promote myelin formation and repair. *Nat. Rev. Neurol.* **6**, 276–287 (2010).
4. A. L. Herbert, K. R. Monk, Advances in myelinating glial cell development. *Curr. Opin. Neurobiol.* **42**, 53–60 (2017).
5. Y. Miyamoto, J. Yamauchi, Recent insights into molecular mechanisms that control growth factor receptor-mediated Schwann cell morphological changes during development, in *Schwann Cell Development and Pathology*, K. Sango, J. Yamauchi, Eds. (Springer, 2014), chap. 2, pp. 5–27.
6. R. A. Kahn, J. Cherfils, M. Elias, R. C. Lovering, S. Munro, A. Schurmann, Nomenclature for the human Arf family of GTP-binding proteins: ARF, ARL, and SAR proteins. *J. Cell Biol.* **172**, 645–650 (2006).
7. C. D'Souza-Schorey, P. Chavrier, ARF proteins: Roles in membrane traffic and beyond. *Nat. Rev. Mol. Cell Biol.* **7**, 347–358 (2006).
8. J. E. Casanova, Regulation of Arf activation: The Sec7 family of guanine nucleotide exchange factors. *Traffic* **8**, 1476–1485 (2007).
9. J. G. Donaldson, C. L. Jackson, ARF family G proteins and their regulators: Roles in membrane transport, development, and disease. *Nat. Rev. Mol. Cell Biol.* **12**, 362–375 (2011).
10. A. Schmidt, A. Hall, Guanine nucleotide exchange factors for Rho GTPases: Turning on the switch. *Genes Dev.* **16**, 1587–1609 (2002).
11. K. L. Rossman, C. J. Der, J. Sondek, GEF means go: Turning on RHO GTPases with guanine nucleotide-exchange factors. *Nat. Rev. Mol. Cell Biol.* **6**, 167–180 (2005).
12. J. Yamauchi, Y. Miyamoto, T. Torii, S. Takashima, K. Kondo, K. Kawahara, N. Nemoto, J. R. Chan, G. Tsujimoto, A. Tanoue, Phosphorylation of cytohesin-1 by Fyn is required for initiation of myelination and the extent of myelination during development. *Sci. Signal.* **5**, ra69 (2012).
13. Y. Miyamoto, N. Yamamori, T. Torii, A. Tanoue, J. Yamauchi, Rab35, acting through ACAP2 switching off Arf6, negatively regulates oligodendrocyte differentiation and myelination. *Mol. Biol. Cell* **25**, 1532–1542 (2014).
14. M. Akiyama, H. Hasegawa, T. Hongu, M. A. Frohman, A. Harada, H. Sakagami, Y. Kanaho, *Trans*-regulation of oligodendrocyte myelination by neurons through small GTPase Arf6-regulated secretion of fibroblast growth factor-2. *Nat. Commun.* **5**, 4744 (2014).
15. T. Torii, Y. Miyamoto, K. Tago, K. Sango, K. Nakamura, A. Sanbe, A. Tanoue, J. Yamauchi, Arf6 guanine nucleotide exchange factor cytohesin-2 binds to CCDC120 and is transported along neurites to mediate neurite growth. *J. Biol. Chem.* **289**, 33887–33903 (2014).
16. J. S. Bonifacino, Adaptor proteins involved in polarized sorting. *J. Cell Biol.* **204**, 7–17 (2014).
17. X. Ren, G. G. Farías, B. J. Canagarajah, J. S. Bonifacino, J. H. Hurley, Structural basis for recruitment and activation of the AP-1 clathrin adaptor complex by Arf1. *Cell* **152**, 755–767 (2013).
18. A. Galindo, N. Soler, S. H. McLaughlin, M. Yu, R. L. Williams, S. Munro, Structural insights into Arl1-mediated targeting of the Arf-GEF BIG1 to the *trans*-Golgi. *Cell Rep.* **16**, 839–850 (2016).
19. T. Shiba, M. Kawasaki, H. Takatsu, T. Nogi, N. Matsugaki, N. Igarashi, M. Suzuki, R. Kato, K. Nakayama, S. Wakatsuki, Molecular mechanism of membrane recruitment of GGA by ARF in lysosomal protein transport. *Nat. Struct. Biol.* **10**, 386–393 (2003).
20. J. B. Sáenz, W. J. Sun, J. W. Chang, J. Li, B. Bursulaya, N. S. Gray, D. B. Haslam, Golgicide A reveals essential roles for GBF1 in Golgi assembly and function. *Nat. Chem. Biol.* **5**, 157–165 (2009).
21. L. P. Jackson, Structure and mechanism of COPI vesicle biogenesis. *Curr. Opin. Cell Biol.* **29**, 67–73 (2014).
22. M. Jaegle, M. Ghazvini, W. Mandemakers, M. Piirsoo, S. Driegen, F. Levavasseur, S. Raghoenath, F. Grosveld, D. Meijer, The POU proteins Brn-2 and Oct-6 share important functions in Schwann cell development. *Genes Dev.* **17**, 1380–1391 (2003).
23. M. L. Feltri, M. D'Antonio, S. Previtali, M. Fasolini, A. Messing, L. Wrabetz, P_0-*Cre* transgenic mice for inactivation of adhesion molecules in Schwann cells. *Ann. N. Y. Acad. Sci.* **883**, 116–123 (1999).
24. M. C. Brown, M. Besio Moreno, E. R. Bongarzone, P. D. Cohen, E. F. Soto, J. M. Pasquini, Vesicular transport of myelin proteolipid and cerebroside sulfates to the myelin membrane. *J. Neurosci. Res.* **35**, 402–408 (1993).
25. E.-M. Krämer, A. Schardt, K.-A. Nave, Membrane traffic in myelinating oligodendrocytes. *Microsc. Res. Tech.* **52**, 656–671 (2001).
26. A. Niemann, P. Berger, U. Suter, Pathomechanisms of mutant proteins in Charcot-Marie-Tooth disease. *Neuromolecular Med.* **8**, 217–242 (2006).
27. R. P. Bunge, Expanding roles for the Schwann cell: Ensheathment, myelination, trophism and regeneration. *Curr. Opin. Neurobiol.* **3**, 805–809 (1993).
28. J. R. Chan, C. Jolicoeur, J. Yamauchi, J. Elliott, J. P. Fawcett, B. K. Ng, M. Cayouette, The polarity protein Par-3 directly interacts with $p75^{NTR}$ to regulate myelination. *Science* **314**, 832–836 (2006).
29. T. Torii, N. Ohno, Y. Miyamoto, K. Kawahara, Y. Saitoh, K. Nakamura, S. Takashima, H. Sakagami, A. Tanoue, J. Yamauchi, Arf6 guanine-nucleotide exchange factor cytohesin-2 regulates myelination in nerves. *Biochem. Biophys. Res. Commun.* **460**, 819–825 (2015).
30. T. Torii, Y. Miyamoto, M. Yamamoto, K. Ohbuchi, H. Tsumura, K. Kawahara, A. Tanoue, H. Sakagami, J. Yamauchi, Arf6 mediates Schwann cell differentiation and myelination. *Biochem. Biophys. Res. Commun.* **465**, 450–457 (2015).
31. B. Yu, I. R. S. Martins, P. Li, G. K. Amarasinghe, J. Umetani, M. E. Fernandez-Zapico, D. D. Billadeau, M. Machius, D. R. Tomchick, M. K. Rosen, Structural and energetic mechanisms of cooperative autoinhibition and activation of Vav1. *Cell* **140**, 246–256 (2010).
32. K. Verhoeven, P. De Jonghe, T. Van de Putte, E. Nelis, A. Zwijsen, N. Verpoorten, E. De Vriendt, A. Jacobs, V. Van Gerwen, A. Francis, C. Ceuterick, D. Huylebroeck, V. Timmerman, Slowed conduction and thin myelination of peripheral nerves associated with mutant Rho guanine-nucleotide exchange factor 10. *Am. J. Hum. Genet.* **73**, 926–932 (2003).
33. V. Delague, A. Jacquier, T. Hamadouche, Y. Poitelon, C. Baudot, I. Boccaccio, E. Chouery, M. Chaouch, N. Kassouri, R. Jabbour, D. Grid, A. Mégarbané, G. Haase, N. Lévy, Mutations in *FGD4* encoding the Rho GDP/GTP exchange factor FRABIN cause autosomal recessive Charcot-Marie-Tooth type 4H. *Am. J. Hum. Genet.* **81**, 1–16 (2007).
34. C. Stendel, A. Roos, T. Deconinck, J. Pereira, F. Castagner, A. Niemann, J. Kirschner, R. Korinthenberg, U.-P. Ketelsen, E. Battaloglu, Y. Parman, G. Nicholson, R. Ouvrier, J. Seeger, P. De Jonghe, J. Weis, A. Krüttgen, S. Rudnik-Schöneborn, C. Bergmann, U. Suter, K. Zerres, V. Timmerman, J. B. Relvas, J. Senderek, Peripheral nerve demyelination caused by a mutant Rho GTPase guanine nucleotide exchange factor, frabin/FGD4. *Am. J. Hum. Genet.* **81**, 158–164 (2007).
35. V. L. Sheen, V. S. Ganesh, M. Topcu, G. Sebire, A. Bodell, R. S. Hill, P. E. Grant, Y. Y. Shugart, J. Imitola, S. J. Khoury, R. Guerrini, C. A. Walsh, Mutations in *ARFGEF2* implicate vesicle trafficking in neural progenitor proliferation and migration in the human cerebral cortex. *Nat. Genet.* **36**, 69–76 (2004).
36. Y. Miyamoto, T. Torii, A. Tanoue, J. Yamauchi, VCAM1 acts in parallel with CD69 and is required for the initiation of oligodendrocyte myelination. *Nat. Commun.* **7**, 13478 (2016).

Acknowledgments: We thank Y. Matsubara, H. Saitoh, and A. Umezawa (National Research Institute for Child Health and Development) for the insightful comments they provided throughout this study. We also thank M. Itaoka for technical assistance for immunoblotting. **Funding:** This work was supported by Grants-in-Aid (nos. 17H03564 and 17K07127) and Branding projects (209001) for Scientific Research from the Japanese Ministry of Education, Culture, Sports, Science and Technology. This work was also supported by Grants-in-Aid (nos. 26-2 and 27-2) for Medical Scientific Research from the Japanese Ministry of Health, Labor, and Welfare. This work was partially supported by the Astellas Foundation.
Author contributions: Conceptualization: Y.M. and J.Y. Data curation: Y.M. and T.T. Investigation: Y.M., T.T., K.T., A.T., and S.T. Methodology: Y.M. and T.T. Writing the original draft, review, and editing: Y.M. and J.Y. **Competing interests:** The authors declare that they have no competing interests. **Data and materials availability:** All data needed to evaluate the conclusions in the paper are present in the paper and/or the Supplementary Materials. Additional data related to this paper may be requested from the authors.

Submitted 8 November 2017
Accepted 20 February 2018
Published 4 April 2018
10.1126/sciadv.aar4471

Citation: Y. Miyamoto, T. Torii, K. Tago, A. Tanoue, S. Takashima, J. Yamauchi, BIG1/Arfgef1 and Arf1 regulate the initiation of myelination by Schwann cells in mice. *Sci. Adv.* **4**, eaar4471 (2018).